Biochemistry

pubs.acs.org/biochemistry Article

# *Danio rerio* Oocytes for Eukaryotic In-Cell NMR

Joseph F. Thole, Tanner C. Fadero, Jeffrey P. Bonin, Samantha S. Stadmiller, Jonathan A. Giudice, and Gary J. Pielak*

Cite This: *Biochemistry* 2021, 60, 451−459 Read Online

ACCESS | Metrics & More | Article Recommendations | Supporting Information

**ABSTRACT:** Understanding how the crowded and complex cellular milieu affects protein stability and dynamics has only recently become possible by using techniques such as in-cell nuclear magnetic resonance. However, the combination of stabilizing and destabilizing interactions makes simple predictions difficult. Here we show the potential of *Danio rerio* oocytes as an in-cell nuclear magnetic resonance model that can be widely used to measure protein stability and dynamics. We demonstrate that in eukaryotic oocytes, which are 3−6-fold less crowded than other cell types, attractive chemical interactions still dominate effects on protein stability and slow tumbling times, compared to the effects of dilute buffer.

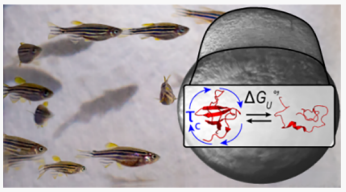




For more than a century, biochemistry focused on the properties of proteins and other macromolecules in buffer alone. Recently, investigators have begun to explore proteins[1−3] and RNA[4,5] in the environment where they evolved: in the cell. This crowded and complex milieu is predicted to stabilize proteins and their complexes due to hard-core repulsions,[6] although shape also plays a role.[7−9] Simultaneously, soft interactions—charge−charge, dipole, nonpolar, and others—can be stabilizing or destabilizing, depending on whether they are repulsive or attractive, respectively.[10] While it is easy to advocate measurements in cells, realistically, these are challenging endeavors requiring a large investment of both time and supplies. Our goal is to develop simple, practical, and economical systems that are broadly applicable to a variety of questions about the effect of the cellular interior on proteins.

Quantifying in-cell biochemistry of specific target proteins requires a label. Fluorescence microscopy is commonly used for studying macromolecular localization, abundance, dynamics, and interactions.[11−14] These efforts provide key insight into how the cellular environment impacts the tertiary and quaternary structure and changes in macromolecular assemblies. However, a potential drawback is that most of these efforts rely on the introduction of large (0.1 to >10 kDa) fluorescent labels. These labels can potentially interfere with the behavior of the protein being studied.[15]

Nuclear magnetic resonance spectroscopy (NMR) avoids large labels while providing atomic-resolution information about the structure, stability, and dynamics of macromolecules in living cells.[5,16−23] Serber et al.[16] showed the utility of *Escherichia coli* as a model organism for in-cell NMR because strains optimized for recombinant protein expression are useful for enriching proteins with NMR-active nuclei and allow observation of target proteins in the sea of other cellular molecules. However, many proteins are difficult or impossible to observe by in-cell NMR in *E. coli* because surface residues make nonspecific contacts with other macromolecules, slowing their tumbling and broadening their resonances into the background.[24−26]

This disappearance of target protein signals in *E. coli* and some eukaryotic cells emphasizes the need for systems that allow a larger range of macromolecules to be assessed. Several techniques have been employed to introduce isotopically enriched or labeled proteins into eukaryotic cells, including electroporation,[20,27] importation tags,[18] expression,[18,28,29] and pore-forming toxins.[30] These methodologies, however, do not allow facile access to, and accurate control of, target protein concentration, a property critical for the future quantification of protein−protein interactions.[31,32]

Selenko et al.[17] bypassed these limitations by microinjecting the model B1 domain of the streptococcal immunoglobulin G-binding protein (GB1) into *Xenopus laevis* oocytes. Oocytes are useful for studying the effects of the cytoplasmic milieu on proteins because they are fixed in development, which minimizes changes due to the cell cycle and growth.[33,34] Sánchez-López et al. used transparent early stage *Danio rerio* (zebrafish) embryos to assess enzyme activity *in vivo*.[35] To exploit the transparency of zebrafish, while maintaining the stable cellular environment, we employ unfertilized zebrafish oocytes to assess their utility for in-cell NMR. Here, we validate the detectability and cytoplasmic location of a test protein (Figure 1), the 7 kDa N-terminal src homology 3 domain (SH3) domain of the *Drosophila melanogaster* signal transduction protein Drk, and then quantify its stability and dynamics.

**Received:** November 24, 2020
**Revised:** January 7, 2021
**Published:** February 3, 2021






https://dx.doi.org/10.1021/acs.biochem.0c00922
*Biochemistry* 2021, 60, 451−459

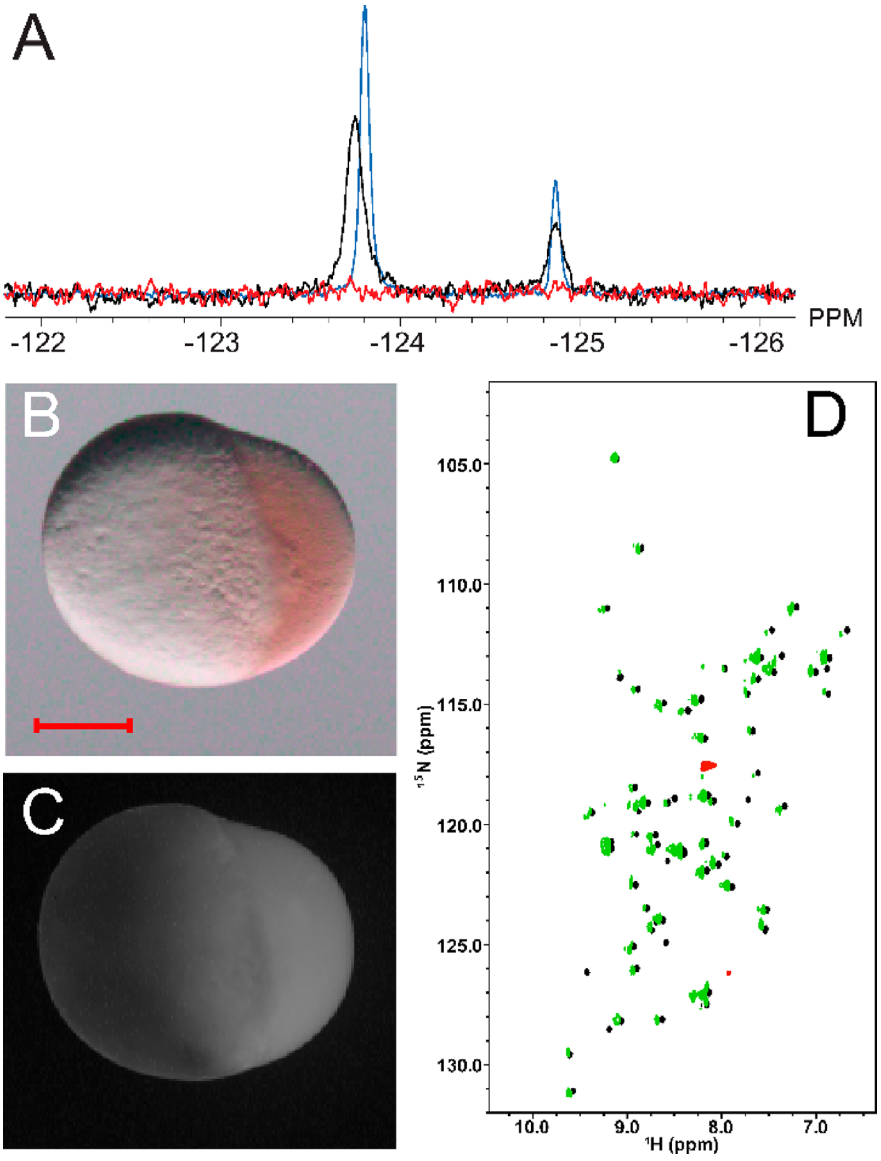


**Figure 1.** (A) Representative $^{19}$F NMR spectra at 298 K of $^{19}$F-labeled wild-type SH3 in buffer (blue), in oocytes (black), and in the 2:1 dilution leakage control (red). The folded state and unfolded state chemical shifts are at approximately −123.7 and −124.85 ppm, respectively. (B) Bright-field image of a *D. rerio* oocyte injected with 1 mM T22G;C60 SH3 covalently tagged with bromobimane. The scale bar is 200 $\mu$m. (C) Same oocyte imaged with epifluorescence (excitation from 436 to 420 nm, emission from 480 to 440 nm). (D) $^{15}$N−$^{1}$H HSQC spectra of $^{15}$N-enriched T22G SH3 in *D. rerio* oocytes (green, 62.5 $\mu$M), *E. coli* (red, ∼1 mM), and buffer at pH 7.5 (black, 490 $\mu$M). The solution surrounding the oocytes was interrogated by NMR, but no SH3 resonances were observed.

## MATERIALS AND METHODS

**Protein Preparation.** Fluorine-labeled SH3 was prepared as described,[36−38] except that expression was allowed to proceed for 12−14 h at 18.5 °C. Fluorine-labeled N51K SH3 was expressed in the same way, except it was cloned into a pET28b (Novagen) vector with an N-terminal hexahistidine and SUMO tags, transformed into BL21 Star (DE3) One Shot cells (Invitrogen). cOmplete Protease Inhibitor Cocktail (Protease Inhibitors, Roche) was added to the cell pellets, and the samples were sonicated (Fisher Scientific Sonic Dismembrator model 500, 20% amplitude, 0.4 s on, 0.2 s off, 15 min). Protease inhibitors were added again, and the lysates centrifuged (Sorvall RC-5B, 17540 rcf, 4 °C, 45 min) and then syringe filtered (0.45 $\mu$m, Millex).

Lysates were processed by FPLC (ÄKTA pure) using a $Ni^{2+}$ column (Cytiva HisTrap HP) pre-equilibrated with loading buffer [15.1 mM $Na_2HPO_4$, 4.9 mM $NaH_2PO_4$, 500 mM NaCl, and 20 mM imidazole (pH 8)]. The column was washed with 50 mL of loading buffer. The protein was eluted with 15.1 mM $Na_2HPO_4$, 4.9 mM $NaH_2PO_4$, 500 mM NaCl, and 200 mM imidazole (pH 8). Fractions of interest were combined with Cth protease (final concentration 1−2 nM).[39] Digestion proceeded while the sample was dialyzed against 50 mM $Na_2HPO_4$, 20 mM $NaH_2PO_4$, and 9 mM NaCl for 4−6 h. The digested sample was subjected to $Ni^{2+}$ chromatography as described above. The flow-through was collected, and the protein further purified using size-exchange and hydrophobic interaction chromatography.[36] The purity was assessed by using sodium dodecyl sulfate−polyacrylamide gel electrophoresis (SDS−PAGE) and mass spectrometry (Thermo Q Exactive HF-X, SH3, 6877.6 Da expected, 85% 6873.3 Da and 15% 6855.3 observed; N51K SH3, 6891.7 Da expected, 90%


https://dx.doi.org/10.1021/acs.biochem.0c00922
*Biochemistry* 2021, 60, 451−459

6891.2 Da and 10% 6873.4 Da observed) and $^{19}$F NMR. The lower-mass species are not $^{19}$F-labeled. Wild-type SH3 yielded 3−6 mg of purified protein/L of culture. N51K SH3 yielded 6−10 mg/L.

Purified samples were buffer exchanged using PD-10 desalting columns (Cytiva) into *D. rerio* Ringer's solution [116 mM NaCl, 2.9 mM KCl, 1.8 mM $CaCl_2$, and 5 mM Hepes (pH 7.4)].[40] SH3 was concentrated to >13 mM using a Millipore Amicon Ultra concentrator (3 kDa cutoff). Protease inhibitors were added to a final concentration of 10×, and phenyl red dye was added to a level of 0.5% (w/v). Final protein concentrations were 11.3 mM for SH3 and 13.4 mM for N51K SH3. Samples were flash-frozen and stored at −80 °C.

$^{15}$N-enriched K10H GB1, $^{15}$N-enriched and $^{19}$F-labeled T22G SH3, and T22G/C60 SH3 were prepared as described,[1,41] and their purity was validated by SDS−PAGE and mass spectrometry (K10H GB1, 6300.3 Da expected, 6296.8 Da observed; T22G SH3, 6903.97 Da expected, 86.7% 6904.0 Da and 11.4% 6886.5 Da observed). The T22G/C60 SH3 variant was prepared as described above, except that 1 mM dithiothreitol was added to buffers (6918.6 Da expected, 6918.3 Da observed). Samples were flash-frozen and lyophilized for storage. Prior to injection, the proteins were dissolved in *D. rerio* Ringer's solution with 10× protease inhibitors containing 0.5% phenyl red (final concentration).

**Bromobimane Fluorescence.** T22G;C60 SH3 was mixed with bromobimane at a 1:10 molar ratio in 15.1 mM $Na_2HPO_4$, 4.9 mM $NaH_2PO_4$, 150 mM NaCl, and 5 mM EDTA (pH 7.6). The reaction was allowed to proceed for 12 h at 4 °C. The protein was separated from unreacted dye by using a PD-10 column and exchanged into $H_2O$ for lyophilization.

**Zebrafish Oocyte Injections.** AB strain adult female zebrafish were set up in breeding tanks 1 day prior to experiments. The following morning, the fish were anesthetized in 0.08% Tricaine (3-aminobenzoic acid ethyl ester) in E3 (5 mM NaCl, 170 μM KCl, 330 μM $CaCl_2$, 330 μM $MgSO_4$, and 0.00003% methylene blue).[40] Oocytes were gently squeezed from the fish using a plastic spoon to distribute the force. Dead or misshapen oocytes were removed. Oocytes were loaded onto 3% agarose plates for injection when a prominent blastodisc was observed (∼25 min).

The protein injection solution was loaded into the back of a glass capillary needle. The point of the needle was clipped. The air injection system (Parker Picospritzer III) was set to 30 psi. The injection bubble diameter, 210 μm, measured in mineral oil using a stage micrometer, corresponds to a 4.5 nL injection. Injections were made through the yolk to just below, or into, the blastodisc. Assuming a cytoplasmic volume of 50 nL (see Microscopy), the final cytoplasmic concentration of injected protein was 1.2−1.4 mM.[17]

Five hundred to seven hundred oocytes were injected per trial. The oocytes were allowed to recover in E3 in a 55 mm Petri dish for at least 1 h. Oocytes damaged by injection, or those in which the injection solution was not taken into the cytoplasm (e.g., phenyl red localized in the yolk, rather than the blastodisc), were removed. Between 300 and 550 of the healthiest-looking oocytes were transferred to E3 and 1.5% Ficoll 70 (Sigma) (pH 7.5). This Ficoll concentration compressed the blastodisc within 30 min without damaging the oocytes. Oocytes were transferred to a Shigemi NMR tube, prefilled with E3 and 1.5% Ficoll 70 (pH 7.5) to prevent damage to the injected oocytes. The total number of oocytes added to the tube was recorded, and additional solution was removed until the volume was 350 μL. The solution was then adjusted to E3, 1.5% Ficoll 70, and 10% $D_2O$ using E3, 1.5% Ficoll 70, and 90% $D_2O$, at a pH meter reading of 7.5. This study was carried out under the UNC-CH Institutional Animal Care & Use Committee under Protocol 18-004.0.

**Comments on Injection.** There are three primary determinants for successful injections. The most important determinant is oocyte quality. An unhealthy fish yields few, if any, healthy oocytes. Additionally, the first two or three collections from a newly mature fish or a multiweek break in laying can result in poor quality oocytes. The second determinant comprises the injection parameters. An injection air pressure between 20 and 30 psi maximizes the injection volume without damaging the oocyte, and a narrow needle minimizes oocyte damage. The third factor is the operator's skill. Novices learning needle placement have a success rate of ∼50%, which reaches 80−90% with experience.

**Identifying Dead Oocytes and Leakage Controls.** NMR tubes were inspected for dead oocytes after each data acquisition. Dead oocytes are bright white and therefore quickly counted. Data were rejected if ≥10% of the oocytes died. To assess leakage, the solution surrounding the oocytes was removed using a Pasteur pipet. The volume was measured and adjusted to 350 μL with E3, 1.5% Ficoll 70, and 10% $D_2O$. The leak-check sample was subjected to the same acquisition parameters as the oocyte sample at 298 K. Signals from the protein of interest were not detected.

**Microscopy.** The preparation, collection, and injection of zebrafish oocytes were carried out as described above. Lyophilized, T22G SH3, and bromobimane-labeled T22G;C60 SH3 were resuspended in Ringer's solution with phenyl red to give a final protein concentration of 10 mM. The final intracellular protein concentration was ∼1 mM. Additional injections were made using only Ringer's solution with phenyl red. Epifluorescence images (Figure 1B,C and Figure S1) were acquired using an Axiozoom.V16 stereomicroscope (Zeiss) equipped with an Axiocam 503 color (Zeiss) after allowing injected oocytes to recover in E3 for 1 h (excitation from 436 to 420 nm, emission from 480 to 440 nm). Oocytes were placed on a 150 mm Petri dish for imaging, with chorions mechanically removed with forceps.

Cytoplasmic volume estimates were made by imaging 30 fully segregated oocytes (≥4 h after collection) using a model M205FA stereomicroscope (Leica) equipped with a model DFC360FX camera (Leica). The methodology was adapted from ref 42. Ovals were drawn over the blastodisc and yolk region using Adobe Illustrator. Oval radii were measured in the vertical and horizontal directions. The cytoplasm and yolk were assumed to be half-spheroids. When the yolk occupied a portion of the cytoplasmic volume, the yolk volume was subtracted from the cytoplasmic volume (Figure S2).

Laser-scanning confocal microscopy (LSCM) was used to observe the redistribution of injected bromobimane-labeled T22G;C60 SH3. Injections were performed as described above. The final intracellular protein concentration was 0.5 mM. A model LU-N4/N4S (Nikon Instruments, Inc.) laser combiner, an acousto-optical tunable filter, and a solid state, 15 mW, 405 nm laser (25% intensity) were used to excite the bromobimane label. An A1R galvanometric mirror confocal scan head (Nikon Instruments, Inc.) operated in "galvo mode" was used to scan the excitation light and descan the emission


https://dx.doi.org/10.1021/acs.biochem.0c00922
Biochemistry 2021, 60, 451−459

light through a 90.67 μm hexagonal pinhole (physical size). An inverted 10× CFI Plan Fluor air-immersion 0.3 NA objective-type lens element (Nikon Instruments, Inc.) was used to deliver the scanned excitation light and collect the emission light through a #1.5 glass coverslip in a closed-top chamber to prevent the evaporation of media. The dimensions of the captured images were 1024 pixels × 1024 pixels at a pixel size of 1.243 μm. A three-dimensional volume was acquired using 35 optical slices at 15 μm step sizes via an objective Ti ZDrive (Nikon Elements). The fluorescence was detected through a 450/50 filter cube (Chroma Technology Corp.) using a Multi-Alkali photomultiplier tube housed in a A1-DUG-2 Multi Detector Unit (Nikon Instruments, Inc.). Images were acquired, and three-dimensional reconstructions were made using NIS-Elements acquisition software (Nikon Instruments, Inc.).

**NMR Acquisition.** Data were processed using Topspin 3.6.2. Measurements were taken on Bruker Avance III HD spectrometers equipped with QCI cryoprobes ($^1$H Larmor frequencies of 500 or 600 MHz, or 470 or 564 MHz, respectively, for $^{19}$F) or TCI cryoprobes ($^1$H Larmor frequencies of 700 or 850 MHz). $^{19}$F measurements (Figure 1A and Figure S3) comprised 280 scans of a 7000 Hz sweep width and 7000 points per acquisition with a relaxation delay of 4 s. Measurements were taken from 301 to 286 K for in-cell experiments and from 318 to 280 K for *in vitro* experiments with equilibration times of 10 min (Figure 2). For in-cell experiments with the SH3 N51K variant, 80 pulses were added to each progressive temperature point. Buffer measurements were taken in Ringer's solution with 10% $D_2O$ and 0.05% phenyl red (w/v) (pH 7.4) with $^{19}$F-labeled SH3 and N51K SH3 concentrations of 0.2−0.3 mM. The reversibility was shown by returning to 298 K at the end of each buffer experiment (stability within 10%). $^{15}$N−$^1$H HSQC spectra of the T22G SH3 variant in oocytes were acquired with 13600 and 3000 Hz sweep widths in the $^1$H and $^{15}$N dimensions, respectively, and 128 increments of 20 acquisitions at a $^1$H Larmor frequency of 850 MHz.

The 500 MHz HSQC spectra in *E. coli* were acquired with sweep widths of 8000 and 2280 Hz in the $^1$H and $^{15}$N dimensions, respectively, and 130 indirect increments of 32 acquisitions. To assess leakage, cells were gently centrifuged and the measurement was repeated on the supernatant. No signals from our proteins of interest were detected (Figure S4).

To acquire the pH titration curve, $^{15}$N-enriched K10H GB1[43] was dissolved in modified *D. rerio* Ringer's solution (described above, with the addition of 5 mM bis-tris propane and 5 mM citrate) at pH values of 6.0, 6.2, 6.6, 7.0, 7.3, 7.7, 7.9, 8.1, 8.4, and 8.7 using a GB1 concentration 0.4 mM. HSQC spectra were acquired using sweep widths of 11200 and 2500 Hz in the $^1$H and $^{15}$N dimensions, respectively, and 128 indirect increments of eight acquisitions at a Larmor frequency of 700 MHz. Spectra were referenced to the invariant ε $^{15}$N−$^1$H Trp43 cross peak.[43]

Intracellular pH measurements were taken following the injection protocol for $^{15}$N-enriched GB1 K10H as described above, with a final cellular concentration of 1 mM. Measurements were taken from 301 to 286 K in 3 K increments. Oocytes were held at each temperature for 30 min to mimic the $^{19}$F NMR wild-type SH3 measurements. $^{15}$N−$^1$H HSQC spectra of the K10H GB1 variant in oocytes were acquired identically, but with a single increment of 264 acquisitions. Spectra were referenced to the invariant ε $^{15}$N−$^1$H Trp43 peak (Figure 3).[43]

$^{19}$F spin−lattice relaxation ($T_1$) times were measured at 292 K using a signal inversion recovery sequence with delay times of 0.00, 0.05, 0.10 (triplicate), 0.25, 0.50, 0.80, 1.00, and 1.500 s. $^{19}$F transverse relaxation ($T_2$) times were measured at 292 K using a Carr−Purcell−Meiboom−Gill (CPMG) sequence with delays of 0.84, 1.69 (triplicate), 3.38, 5.06, 6.75, 9.28, 11.82, 15.19, 19.41, and 25.32 μs in oocytes, and additional delays of 33.75, 46.42, and 63.3 μs for buffer measurements. Effects of chemical exchange were limited by using an effective field of 5000 Hz. Buffer values were acquired using 520 μM solutions of wild-type or N51K SH3. No leakage was detected. Measurements were taken at $^{19}$F Larmor frequencies of both 470 and 564 MHz.

**NMR Processing, Fitting, and Analysis of Uncertainties.** NMR data were analyzed in Topspin 3.6.2 (Bruker). $^{19}$F free induction decays were zero-filled to 64K points and processed with 5 Hz broadening. Integrals were measured manually. Further analysis was performed using MATLAB R2020a. For protein stability measurements, $^{19}$F data were fit to the integrated Gibbs−Helmholtz equation.[44] Uncertainties were analyzed by generating 1000 data sets, resampling from measured values with replacement. Averages and standard deviations represent values from population fits.[45]

Correlation times ($\tau_C$) were fit using the Model Free formalism,[46,47] globally fitting $T_1$ and $T_2$ data measured at $^{19}$F frequencies of 470 and 564 MHz, respectively, with the folded state order parameter ($S^2$) fixed to 0.82 and the effective correlation ($\tau_s$) fixed to 20 ps.[48] To show that the relative changes observed were independent of the absolute values of $S^2$ and $\tau_s$, we fixed the parameters within ranges of 0.5−1.0 and 10−100 ps, respectively (Table S2).

Uncertainties in $T_1$ and $T_2$ values and correlation times ($\tau_C$) values were estimated as described.[2] Briefly, for $T_1$ and $T_2$, the standard deviation from a triplicate measurement was applied to all measurements, and then a Monte Carlo analysis ($N$ = 1000) was performed to estimate a mean and standard deviation. For $\tau_C$, the mean and standard deviations of $T_1$ and $T_2$ were used in a Monte Carlo ($N$ = 1000) analysis to estimate the mean $\tau_C$ and its standard deviation.

## RESULTS AND DISCUSSION

As stated in the introductory section, test protein spectra are often undetectable in cells. To show that SH3 can be observed after microinjection, we compared the signal from $^{15}$N−$^1$H HSQC spectra of the stabilized SH3 T22G variant[49] in *D. rerio* oocytes and *E. coli* (Figure 1D. Almost every backbone and side chain amide cross peak is observed in oocytes, and broadening does not limit identification of nearby cross peaks. This situation contrasts with the spectrum from inside *E. coli*, where only metabolites are observed,[50] but the protein spectrum appears upon lysis and dilution (Figure S4).[51]

The observation of spectra in oocytes and their absence in *E. coli* arise from the potential for chemical interactions in each cytoplasm. Prokaryotes have cytoplasmic protein concentrations of 200−450 g/L,[52,53] resulting in a large number of nonspecific protein−protein interactions that slow protein tumbling.[26,51,54] The concentration of eukaryotic cytoplasmic proteins is approximately half that in *E. coli*.[55] Amphibian and fish oocytes are even more dilute, with concentrations of 30−60 g/L.[53,56−59] This lower concentration makes oocytes an ideal system for in-cell NMR because a broader selection of


https://dx.doi.org/10.1021/acs.biochem.0c00922
Biochemistry 2021, 60, 451−459

**Table 1. Equilibrium Thermodynamic Parameters for SH3 Unfolding**[a]

| | | $T_m$ (K) | $\Delta H_{U,T_m}$ (kcal mol$^{-1}$) | $T_s$ (K) | $\Delta H_{U,T_s}$ (kcal mol$^{-1}$) | $\Delta C_p$ (kcal mol$^{-1}$ K$^{-1}$) |
|---|---|---|---|---|---|---|
| WT | buffer | 310.1 ± 0.3 | 21.6 ± 0.7 | 287.5 ± 0.7 | 0.80 ± 0.01 | 0.92 ± 0.07 |
| | oocytes | 310 ± 1 | 19.4 ± 0.5 | 290 ± 2 | 0.64 ± 0.03 | |
| N51K | buffer | 311.3 ± 0.2 | 23.1 ± 0.6 | 288.5 ± 0.3 | 0.857 ± 0.007 | 0.97 ± 0.04 |
| | oocytes | 309.3 ± 0.5 | 20.2 ± 0.2 | 289.1 ± 0.6 | 0.66 ± 0.02 | |

[a]Uncertainties are the standard deviations of parameter estimates using resampling. See the NMR Processing, Fitting, and Analysis of Uncertainty for details.

macromolecules, in terms of both size and charge, will be quantifiable.

The unfolded population of wild-type SH3 in buffer is significant, even under nondenaturing conditions.[2,37,44,60,61] To measure SH3 stability, we introduced one fluorine atom into its sole tryptophan by adding 5-fluoroindole during expression in *E. coli*.[62,63] SH3 undergoes two-state folding.[60] The rate of exchange between the folded and unfolded states is small relative to the frequency difference of the $^{19}$F resonances from each state (i.e., slow exchange),[2,64] which means the areas of the resonances are directly proportional to their relative concentrations. The stability of the protein can therefore be quantified as the modified (neutral pH) standard state free energy of unfolding, $\Delta G_U^{\circ\prime}$

$$\Delta G_U^{\circ\prime} = -RT \ln \frac{[\text{unfolded population}]}{[\text{folded population}]} \quad (1)$$

where $R$ is the gas constant and $T$ is the absolute temperature. Plotting $\Delta G_U^{\circ\prime}$ as a function of temperature allows us to use the integrated Gibbs–Helmholtz equation (eq 2) to estimate the modified standard state enthalpy ($\Delta H_U^{\circ\prime}$), entropy ($\Delta S_U^{\circ\prime}$), and heat capacity ($\Delta C_p^{\circ\prime}$) of unfolding at a reference temperature ($T_{ref}$).[65] This model assumes that $\Delta C_p$ is constant over the narrow temperature range tested.[65,66]

$$\Delta G_U^{\circ\prime} = H_U^{\circ\prime} - T\Delta S_U^{\circ\prime} + \Delta C_p^{\circ\prime}\left(T - T_{ref} - T \ln \frac{T}{T_{ref}}\right) \quad (2)$$

We measured SH3 stability as a function of temperature in buffer and oocytes (Figure 2, Table 1). Due to viability limitations, measurements were confined to the range of 286–301 K. This choice limited our ability to quantify $\Delta C_p$, but we expected small changes to this parameter in cells and therefore used the buffer value[2] to fit the in-cell data.

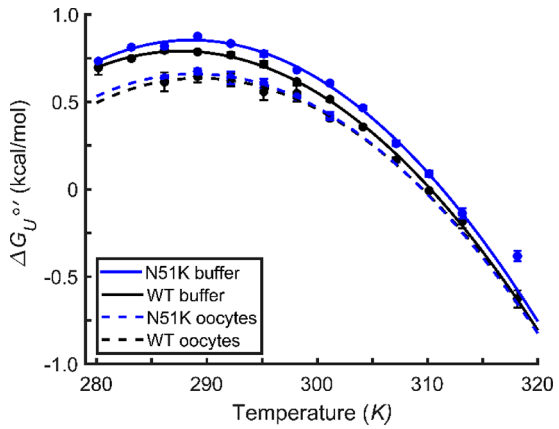


**Figure 2.** Temperature dependence of the stability of wild-type (WT) SH3 and the N51K variant in buffer (pH 7.5) and *D. rerio* oocytes. Averages and standard errors of the mean are shown along with fits to eq 2.

SH3 is less stable in oocytes than in buffer. The destabilization is enthalpically driven (Table 1 and Figure S5) because the temperature of maximum stability ($T_s$) is unchanged from the buffer value, but $\Delta H_{T_s}^{\circ\prime}$ decreases. Additionally, the melting temperature ($T_m$) remains constant while $\Delta H_{U,T_m}^{\circ\prime}$ decreases. The decreased stability is caused by attractive chemical interactions between the surface of SH3 and the cellular milieu.[67,68] These attractive interactions are destabilizing because protein unfolding exposes additional surface that is attractive to the cellular milieu. This decreased stability in oocytes is smaller in magnitude but similar in direction to the destabilization of the same protein in *E. coli*.[2] The observation that the more crowded *E. coli* cytoplasm and the less crowded oocyte cytoplasm are both destabilizing indicates that chemical interactions may be more important than hard-core repulsions in cells.

Destabilizing attractive contacts include charge–charge interactions. The average net charge of *D. rerio* oocyte proteins is negative at physiological pH,[69,70] as it is in prokaryotes,[71] while SH3 has a net charge of −6. Simple analyses based on steric and net charge repulsion predict that SH3 should be stabilized in cells compared to buffer. The destabilization shows the importance of these other attractive interactions in cells.

Nevertheless, charge still plays a key role as shown by our studies of the N51K variant, which changes the charge by +1 (Table 1 and Figure S6). Given the net negative protein charge in cells, this change should further destabilize SH3 in cells compared to buffer by increasing the number of attractive interactions. This prediction is supported; the variant is more destabilized ($\Delta\Delta G_U^{\circ\prime}$) at $T_s$ than in the wild-type protein. We attempted to study other charge change variants (see the Supporting Information). They were prone to aggregation, were clogging the needle, or did not follow two-state folding in oocytes.

Another important concern is diffusion. Several measurements have been reported in biologically relevant crowders *in vitro*,[72,73] in *E. coli*,[22,74] and in *X. laevis* oocytes.[22] We estimated the relative viscosity in zebrafish oocytes by measuring the ratio of the rotational correlation time ($\tau_C$, eq 3) in oocytes compared to that in buffer.

$$\tau_C = \frac{6\eta V}{k_B T} \quad (3)$$

where $k_B$ is the Boltzmann constant, $\eta$ is the viscosity (kg s m$^{-1}$), and $V$ is the volume of SH3 (m$^3$), which is known.[73] Given that the cellular environment is unlikely to change the shape of a folded globular protein, the ratio of $\tau_C$ values equals the ratio of viscosities. $\tau_C$ was estimated via the Model-Free


https://dx.doi.org/10.1021/acs.biochem.0c00922
Biochemistry 2021, 60, 451–459

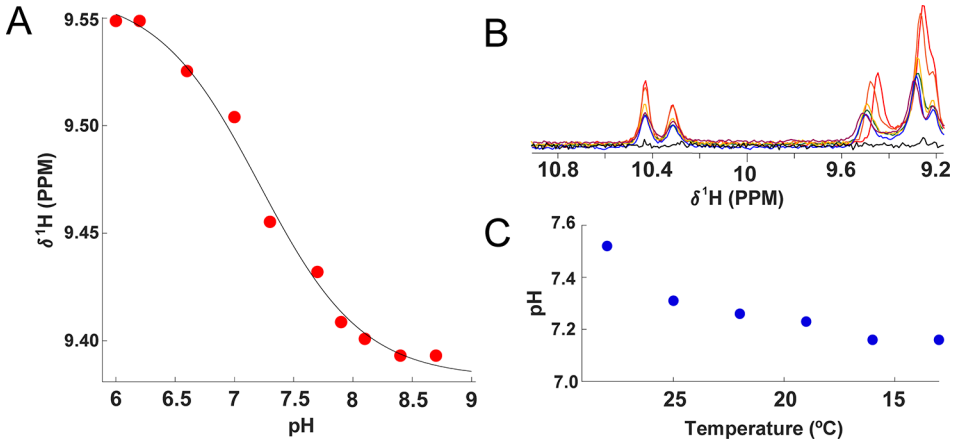


**Figure 3.** pH of the *D. rerio* oocyte cytoplasm. (A) Standard curve of histidine 10 $^{1}$H chemical shifts of K10H GB1 at varying pH values (298 K) in buffer. (B) $^{15}$N−$^{1}$H spectra of K10H GB1 injected into zebrafish oocytes at 301 K (red), 298 K (orange), 295 K (yellow), 292 K (green), 289 K (blue), and 286 K (purple) and a leakage control (black). The histidine 10 resonance is located between 9.5 and 9.4 ppm. The tryptophan 43 $\varepsilon$-$^{15}$N−$^{1}$H resonance at 10.41 ppm was used as a reference for chemical shift calculations. (C) Estimated intracellular pH as a function of temperature while replicating the protocol used for SH3 stability measurements.

approach using spin−lattice and transverse relaxation times (Table 2).[46−48]

**Table 2. Rotational Correlation Times ($\tau_C$, ns per radian) at 292 K of Folded SH3 and Its Variant in Buffer (pH 7.5) and *D. rerio* Oocytes**

| | buffer $\tau_C$[a,b] | in-cell $\tau_C$[a,b] | relative change[c] |
|---|---|---|---|
| WT | 4.4 ± 0.1 | 11 ± 2 | 2.5 ± 0.5 |
| N51K | 5.3 ± 0.1 | 14 ± 3 | 2.6 ± 0.6 |

[a]Order parameter ($S^2$) fixed to 0.82. $\tau_e$ fixed to 20 ns.[48] [b]See the NMR Processing, Fitting, and Analysis of Uncertainty for a discussion of uncertainty. [c]Uncertainties from error propagation.

Both wild-type SH3 and the charge change variant N51K perceive a viscosity that is ∼2.5 times greater in oocytes than in buffer. This ratio is similar to that for a small protein in *X. laevis*, but the viscosity perceived in *E. coli* is ∼7-fold greater than in buffer.[22] The faster diffusion in oocytes compared to *E. coli* reflects the higher macromolecule concentration in bacteria. The similar viscosities of *X. laevis* and zebrafish oocyte cytoplasms indicate that protein diffusion is comparable across oocytes from these two distantly related species. Computational studies support the idea that protein−protein chemical interactions are the primary cause of the increased viscosity compared to that in buffer.[75,76] The observation that changing the charge does not affect the relative viscosity of the wild-type protein and the charge change variant shows that interactions beyond simple electrostatics are important.

We could not quantify the relative viscocity experienced by unfolded SH3 in oocytes because we had to choose a temperature that allowed acquisition of reliable data over the multihour measurement times. At that temperature (293 K), the population of the unfolded state is too small to obtain the requisite data. Increasing the temperature increases the population of the unfolded state and increases the rate of oocyte death.

Another consideration is ensuring that the in-cell environment reflects typical cell function. One measure is intracellular pH ($pH_i$), which is tightly regulated by cells, and alterations are associated with breakdowns in homeostasis.[77,78] Our protein homogeneously occupies the cytoplasm (Figure 1, Figure S1, and Movie S1), and therefore, a similar measure of cytoplasmic $pH_i$ is appropriate. The K10H variant of GB1 has been characterized as an in-cell pH probe.[43] A fit of the H10 $^{15}$N−$^{1}$H cross peak across a range of pH values to the Henderson−Hasselbalch equation yields a p$K_a$ of 7.2 at 25 °C (Figure 3A). We accounted for the temperature dependence of ionization by combining this information with ionization enthalpy values of surface histidines.[79] Using this correction, the p$K_a$ was estimated for each temperature, in the same order of acquisition as was performed for SH3 and N51K SH3 stability measurements (Figure 3C). Initially, the cytoplasm is slightly alkaline relative to a typical eukaryotic cytoplasm $pH_i$,[78] as reported for zebrafish embryos,[80] and then the pH decreases to 7.3−7.2 within 1 h. These data indicate that zebrafish oocytes are a reasonable model for a eukaryotic cytoplasm.

In summary, our results show that destabilizing attractive interactions can outcompete stabilizing repulsive interactions in cells, even when the overall intracellular protein concentration is significantly lower. However, the similar diffusion of the wild-type protein and the charge change variant in oocytes highlights the idea that a broader range of intermolecular interactions, including hydrogen bonding, that have cellular effects on proteins need to be studied.[68]

We also demonstrated that zebrafish oocytes are a viable system for in-cell NMR. *X. laevis* oocytes have been used in several publications.[17,22,81] Over the course of this study, we observed that some injected oocytes fail to incorporate some or all of the test protein into the cytoplasm. The use of phenyl red makes a lack of incorporation easy to detect because zebrafish oocytes are transparent.

We suggest that zebrafish oocytes are robust vehicles for in-cell NMR for several reasons. Their transparency permits validation of injection localization to ensure the NMR signal originates only from the cytoplasm. Furthermore, *D. rerio* is a widely used, lower-cost model organism because of its popularity in genetic, developmental biology and toxicology studies.[82,83] Zebrafish oocyte collection is simpler, and fish have a shorter recovery time (2−3 weeks vs 1−4 months for *X. laevis*), allowing more data to be collected in a shorter time.[40,84,85] Our work demonstrates a simple and effective


https://dx.doi.org/10.1021/acs.biochem.0c00922
Biochemistry 2021, 60, 451−459

method for studying macromolecules and their ligands in cell. The use of zebrafish oocytes makes in-cell NMR more accessible and improves our understanding of protein chemistry in living cells.

## ■ ASSOCIATED CONTENT

### Supporting Information

The Supporting Information is available free of charge at https://pubs.acs.org/doi/10.1021/acs.biochem.0c00922.

Mutagenisis protocol, microscopy controls and representative in-cell NMR spectra with controls (PDF)

Video reconstruction of confocal microscopy images of 0.5 mM fluorescently tagged (with bromobimane) T22G;C60 SH3 localized to the zebrafish cytoplasm (AVI)

### Accession Codes

drk N-terminal SH3 domain, Q6YKA8; immunoglobulin G-binding protein, P06654.

## ■ AUTHOR INFORMATION


### Corresponding Author

**Gary J. Pielak** − *Department of Chemistry, The University of North Carolina at Chapel Hill, Chapel Hill, North Carolina 27599, United States; Department of Biochemistry and Biophysics, Lineberger Comprehensive Cancer Center, and Integrative Program for Biological and Genome Sciences, The University of North Carolina at Chapel Hill, Chapel Hill, North Carolina 27599, United States;* orcid.org/0000-0001-6307-542X; Phone: (919) 962-4495; Email: gary_pielak@unc.edu

### Authors

**Joseph F. Thole** − *Department of Chemistry, The University of North Carolina at Chapel Hill, Chapel Hill, North Carolina 27599, United States*

**Tanner C. Fadero** − *Department of Biology, The University of North Carolina at Chapel Hill, Chapel Hill, North Carolina 27599, United States*

**Jeffrey P. Bonin** − *Department of Biochemistry and Biophysics, The University of North Carolina at Chapel Hill, Chapel Hill, North Carolina 27599, United States*

**Samantha S. Stadmiller** − *Department of Chemistry, The University of North Carolina at Chapel Hill, Chapel Hill, North Carolina 27599, United States*

**Jonathan A. Giudice** − *Department of Chemistry, The University of North Carolina at Chapel Hill, Chapel Hill, North Carolina 27599, United States*

Complete contact information is available at: https://pubs.acs.org/10.1021/acs.biochem.0c00922



### Funding

This work was supported by the National Science Foundation (MCB-1410854, CHE-0922858, CHE-1726291, and MCB-1652512), the United States-Israel Binational Science Foundation (BSF 2017063), the National Institutes of Health (T32 GM008570), and the National Cancer Institute (P30 CA016086).


### Notes

The authors declare no competing financial interest.


## ■ ACKNOWLEDGMENTS

The authors thank members of the Pielak lab, Stuart Parnham, Michelle Altemera, Lauren Kuchenbrod, Jack Prothero, Adam Waterbury, and Marc ter Horst for helpful discussions and Elizabeth Pielak for comments on the manuscript.


## ■ ABBREVIATIONS

SH3, SRC homology 3 domain; GB1, immunoglobulin G-binding protein B1 domain; $pH_i$, intracellular pH; NMR, nuclear magnetic resonance spectroscopy.

## ■ REFERENCES


(1) Monteith, W. B., and Pielak, G. J. (2014) Residue level quantification of protein stability in living cells. *Proc. Natl. Acad. Sci. U. S. A. 111*, 11335−11340.

(2) Smith, A. E., Zhou, L. Z., Gorensek, A. H., Senske, M., and Pielak, G. J. (2016) In-cell thermodynamics and a new role for protein surfaces. *Proc. Natl. Acad. Sci. U. S. A. 113*, 1725−1730.

(3) Feng, R., Gruebele, M., and Davis, C. M. (2019) Quantifying protein dynamics and stability in a living organism. *Nat. Commun. 10*, 1179.

(4) Bao, H.-L., and Xu, Y. (2018) Investigation of higher-order RNA G-quadruplex structures *in vitro* and in living cells by $^{19}F$ NMR spectroscopy. *Nat. Protoc. 13*, 652−665.

(5) Broft, P., Dzatko, S., Krafcikova, M., Hansel-Hertsch, R., Wacker, A., Dötsch, V., Trantirek, L., and Schwalbe, H. (2021) In-cell NMR spectroscopy of functional riboswitch aptamers in eukaryotic cells. *Angew. Chem., Int. Ed. 60*, 865.

(6) Minton, A. P. (2001) The influence of macromolecular crowding and macromolecular confinement on biochemical reactions in physiological media. *J. Biol. Chem. 276*, 10577−10580.

(7) Berg, O. G. (1990) The influence of macromolecular crowding on thermodynamic activity: Solubility and dimerization constants for spherical and dumbbell-shaped molecules in a hard-sphere mixture. *Biopolymers 30*, 1027−1037.

(8) Guseman, A. J., Perez Goncalves, G. M., Speer, S. L., Young, G. B., and Pielak, G. J. (2018) Protein shape modulates crowding effects. *Proc. Natl. Acad. Sci. U. S. A. 115*, 10965−10970.

(9) Graziano, G. (2020) Shape effect on non-covalent dimer stability using classic scaled particle theory. *Chem. Phys. Lett. 743*, 137176.

(10) Guseman, A. J., and Pielak, G. J. (2020) Chapter 12. Protein stability and weak intracellular interactions. In *In-cell NMR spectroscopy: From molecular sciences to cell biology*, pp 188−206, The Royal Society of Chemistry.

(11) Konopka, M. C., Shkel, I. A., Cayley, S., Record, M. T., and Weisshaar, J. C. (2006) Crowding and confinement effects on protein diffusion *in vivo*. *J. Bacteriol. 188*, 6115−6123.

(12) Shi, X., Foo, Y. H., Sudhaharan, T., Chong, S.-W., Korzh, V., Ahmed, S., and Wohland, T. (2009) Determination of dissociation constants in living zebrafish embryos with single wavelength fluorescence cross-correlation spectroscopy. *Biophys. J. 97*, 678−686.

(13) Komatsubara, A. T., Goto, Y., Kondo, Y., Matsuda, M., and Aoki, K. (2019) Single-cell quantification of the concentrations and dissociation constants of endogenous proteins. *J. Biol. Chem. 294*, 6062−6072.

(14) Lerner, E., Cordes, T., Ingargiola, A., Alhadid, Y., Chung, S., Michalet, X., and Weiss, S. (2018) Toward dynamic structural biology: Two decades of single-molecule Förster resonance energy transfer. *Science 359*, eaan1133.

(15) Sukenik, S., Salam, M., Wang, Y., and Gruebele, M. (2018) In-cell titration of small solutes controls protein stability and aggregation. *J. Am. Chem. Soc. 140*, 10497−10503.

(16) Serber, Z., Keatinge-Clay, A. T., Ledwidge, R., Kelly, A. E., Miller, S. M., and Dötsch, V. (2001) High-resolution macromolecular NMR spectroscopy inside living cells. *J. Am. Chem. Soc. 123*, 2446−2447.

(17) Selenko, P., Serber, Z., Gadea, B., Ruderman, J., and Wagner, G. (2006) Quantitative NMR analysis of the protein G B1 domain in *Xenopus laevis* egg extracts and intact oocytes. *Proc. Natl. Acad. Sci. U. S. A. 103*, 11904−11909.
(18) Inomata, K., Ohno, A., Tochio, H., Isogai, S., Tenno, T., Nakase, I., Takeuchi, T., Futaki, S., Ito, Y., Hiroaki, H., and Shirakawa, M. (2009) High-resolution multi-dimensional NMR spectroscopy of proteins in human cells. *Nature 458*, 106−109.
(19) Xu, G., Ye, Y., Liu, X., Cao, S., Wu, Q., Cheng, K., Liu, M., Pielak, G. J., and Li, C. (2014) Strategies for protein NMR in *Escherichia coli*. *Biochemistry 53*, 1971−1981.
(20) Theillet, F. X., Binolfi, A., Bekei, B., Martorana, A., Rose, H. M., Stuiver, M., Verzini, S., Lorenz, D., van Rossum, M., Goldfarb, D., and Selenko, P. (2016) Structural disorder of monomeric α-synuclein persists in mammalian cells. *Nature 530*, 45−50.
(21) Stadmiller, S. S., and Pielak, G. J. (2018) The expanding zoo of in-cell protein NMR. *Biophys. J. 115*, 1628−1629.
(22) Ye, Y., Wu, Q., Zheng, W., Jiang, B., Pielak, G. J., Liu, M., and Li, C. (2018) Quantification of size effect on protein rotational mobility in cells by $^{19}$F NMR spectroscopy. *Anal. Bioanal. Chem. 410*, 869−874.
(23) Tanaka, T., Ikeya, T., Kamoshida, H., Suemoto, Y., Mishima, M., Shirakawa, M., Güntert, P., and Ito, Y. (2019) High-resolution protein 3D structure determination in living eukaryotic cells. *Angew. Chem., Int. Ed. 58*, 7284−7288.
(24) Li, C., Charlton, L. M., Lakkavaram, A., Seagle, C., Wang, G., Young, G. B., Macdonald, J. M., and Pielak, G. J. (2008) Differential dynamical effects of macromolecular crowding on an intrinsically disordered protein and a globular protein: Implications for in-cell NMR spectroscopy. *J. Am. Chem. Soc. 130*, 6310−6311.
(25) Kyne, C., Jordon, K., Filoti, D. I., Laue, T. M., and Crowley, P. B. (2017) Protein charge determination and implications for interactions in cell extracts. *Protein Sci. 26*, 258−267.
(26) Mu, X., Choi, S., Lang, L., Mowray, D., Dokholyan, N. V., Danielsson, J., and Oliveberg, M. (2017) Physicochemical code for quinary protein interactions in *Escherichia coli*. *Proc. Natl. Acad. Sci. U. S. A. 114*, E4556−E4563.
(27) Binolfi, A., Limatola, A., Verzini, S., Kosten, J., Theillet, F.-X., May Rose, H., Bekei, B., Stuiver, M., van Rossum, M., and Selenko, P. (2016) Intracellular repair of oxidation-damaged α-synuclein fails to target C-terminal modification sites. *Nat. Commun. 7*, 10251.
(28) Bertrand, K., Reverdatto, S., Burz, D. S., Zitomer, R., and Shekhtman, A. (2012) Structure of proteins in eukaryotic compartments. *J. Am. Chem. Soc. 134*, 12798−12806.
(29) Banci, L., Barbieri, L., Bertini, I., Luchinat, E., Secci, E., Zhao, Y., and Aricescu, A. R. (2013) Atomic-resolution monitoring of protein maturation in live human cells by NMR. *Nat. Chem. Biol. 9*, 297−299.
(30) Ogino, S., Kubo, S., Umemoto, R., Huang, S., Nishida, N., and Shimada, I. (2009) Observation of NMR signals from proteins introduced into living mammalian cells by reversible membrane permeabilization using a pore-forming toxin, streptolysin O. *J. Am. Chem. Soc. 131*, 10834−10835.
(31) Speer, S. L., Guseman, A. J., Patteson, J. B., Ehrmann, B. M., and Pielak, G. J. (2019) Controlling and quantifying protein concentration in *Escherichia coli*. *Protein Sci. 28*, 1307−1311.
(32) Chu, I. T., Speer, S. L., and Pielak, G. J. (2020) Rheostatic control of protein expression using Tuner cells. *Biochemistry 59*, 733−735.
(33) Nebreda, A. R., and Ferby, I. (2000) Regulation of the meiotic cell cycle in oocytes. *Curr. Opin. Cell Biol. 12*, 666−675.
(34) Tunquist, B. J., and Maller, J. L. (2003) Under arrest: Cytostatic factor (CSF)-mediated metaphase arrest in vertebrate eggs. *Genes Dev. 17*, 683−710.
(35) Sánchez-López, C., Labadie, N., Lombardo, V. A., Biglione, F. A., Manta, B., Jacob, R. S., Gladyshev, V. N., Abdelilah-Seyfried, S., Selenko, P., and Binolfi, A. (2020) An NMR-based biosensor to measure stereospecific methionine sulfoxide reductase activities *in vitro* and *in vivo*. *Chem. - Eur. J. 26*, 14838−14843.
(36) Gorensek-Benitez, A. H., Smith, A. E., Stadmiller, S. S., Perez Goncalves, G. M., and Pielak, G. J. (2017) Cosolutes, crowding, and protein folding kinetics. *J. Phys. Chem. B 121*, 6527−6537.
(37) Stadmiller, S. S., Gorensek-Benitez, A. H., Guseman, A. J., and Pielak, G. J. (2017) Osmotic shock induced protein destabilization in living cells and its reversal by glycine betaine. *J. Mol. Biol. 429*, 1155−1161.
(38) Stadmiller, S. S., and Pielak, G. J. (2018) Enthalpic stabilization of an SH3 domain by $D_2O$. *Protein Sci. 27*, 1710−1716.
(39) Lau, Y. K., Baytshtok, V., Howard, T. A., Fiala, B. M., Johnson, J. M., Carter, L. P., Baker, D., Lima, C. D., and Bahl, C. D. (2018) Discovery and engineering of enhanced SUMO protease enzymes. *J. Biol. Chem. 293*, 13224−13233.
(40) Westerfield, M. (2007) *The zebrafish book. A guide for the laboratory use of zebrafish (Danio rerio)*, 5th ed., University of Oregon Press, Eugene, OR.
(41) Piszkiewicz, S., Gunn, K. H., Warmuth, O., Propst, A., Mehta, A., Nguyen, K. H., Kuhlman, E., Guseman, A. J., Stadmiller, S. S., Boothby, T. C., Neher, S. B., and Pielak, G. J. (2019) Protecting activity of desiccated enzymes. *Protein Sci. 28*, 941−951.
(42) Fuentes, R., and Fernández, J. (2010) Ooplasmic segregation in the zebrafish zygote and early embryo: Pattern of ooplasmic movements and transport pathways. *Dev. Dyn. 239*, 2172−2189.
(43) Cohen, R. D., Guseman, A. J., and Pielak, G. J. (2015) Intracellular pH modulates quinary structure. *Protein Sci. 24*, 1748−1755.
(44) Senske, M., Smith, A. E., and Pielak, G. J. (2016) Protein stability in reverse micelles. *Angew. Chem., Int. Ed. 55*, 3586−3589.
(45) James, G., Witten, D., Haistie, T., and Tibshirani, R. (2013) *An introduction to statistical learning*, 1st ed., Springer-Verlag, New York.
(46) Lipari, G., and Szabo, A. (1982) Model-free approach to the interpretation of nuclear magnetic resonance relaxation in macromolecules. 1. Theory and range of validity. *J. Am. Chem. Soc. 104*, 4546−4559.
(47) Lipari, G., and Szabo, A. (1982) Model-free approach to the interpretation of nuclear magnetic resonance relaxation in macromolecules 2. Analysis of experimental results. *J. Am. Chem. Soc. 104*, 4559−4570.
(48) Farrow, N. A., Zhang, O., Forman-Kay, J. D., and Kay, L. E. (1995) Comparison of the backbone dynamics of a folded and an unfolded SH3 domain existing in equilibrium in aqueous buffer. *Biochemistry 34*, 868−878.
(49) Bezsonova, I., Singer, A., Choy, W. Y., Tollinger, M., and Forman-Kay, J. D. (2005) Structural comparison of the unstable drkN SH3 domain and a stable mutant. *Biochemistry 44*, 15550−15560.
(50) Serber, Z., Ledwidge, R., Miller, S. M., and Dötsch, V. (2001) Evaluation of parameters critical to observing proteins inside living *Escherichia coli* by in-cell NMR spectroscopy. *J. Am. Chem. Soc. 123*, 8895−8901.
(51) Barnes, C. O., Monteith, W. B., and Pielak, G. J. (2011) Internal and global protein motion assessed with a fusion construct and in-cell NMR spectroscopy. *ChemBioChem 12*, 390−391.
(52) Zimmerman, S. B., and Trach, S. O. (1991) Estimation of macromolecule concentrations and excluded volume effects for the cytoplasm of *Escherichia coli*. *J. Mol. Biol. 222*, 599−620.
(53) Theillet, F.-X., Binolfi, A., Frembgen-Kesner, T., Hingorani, K., Sarkar, M., Kyne, C., Li, C., Crowley, P. B., Gierasch, L., Pielak, G. J., Elcock, A. H., Gershenson, A., and Selenko, P. (2014) Physicochemical properties of cells and their effects on intrinsically disordered proteins (IDPs). *Chem. Rev. 114*, 6661−6714.
(54) Crowley, P. B., Chow, E., and Papkovskaia, T. (2011) Protein interactions in the *Escherichia coli* cytosol: An impediment to in-cell NMR spectroscopy. *ChemBioChem 12*, 1043−1048.
(55) Zeskind, B. J., Jordan, C. D., Timp, W., Trapani, L., Waller, G., Horodincu, V., Ehrlich, D. J., and Matsudaira, P. (2007) Nucleic acid and protein mass mapping by live-cell deep-ultraviolet microscopy. *Nat. Methods 4*, 567−569.
(56) Eppig, J. J., Jr., and Dumont, J. N. (1972) Amino acid pools in developing oocytes of *Xenopus laevis*. *Dev. Biol. 28*, 531−536.


https://dx.doi.org/10.1021/acs.biochem.0c00922
*Biochemistry* 2021, 60, 451−459

(57) Masui, Y. (1982) Oscillatory activity of maturation promoting factor (MPF) in extracts of *Rana pipiens* eggs. *J. Exp. Zool. 224*, 389−399.
(58) Lohka, M. J., and Maller, J. L. (1985) Induction of nuclear envelope breakdown, chromosome condensation, and spindle formation in cell-free extracts. *J. Cell Biol. 101*, 518−523.
(59) Taylor, M. A., and Smith, L. D. (1987) Accumulation of free amino acids in growing *Xenopus laevis* oocytes. *Dev. Biol. 124*, 287−290.
(60) Zhang, O., and Forman-Kay, J. D. (1997) NMR studies of unfolded states of an SH3 domain in aqueous solution and denaturing conditions. *Biochemistry 36*, 3959−3970.
(61) Tuinstra, R. L., Peterson, F. C., Kutlesa, S., Elgin, E. S., Kron, M. A., and Volkman, B. F. (2008) Interconversion between two unrelated protein folds in the lymphotactin native state. *Proc. Natl. Acad. Sci. U. S. A. 105*, 5057−5063.
(62) Crowley, P. B., Kyne, C., and Monteith, W. B. (2012) Simple and inexpensive incorporation of $^{19}$F-tryptophan for protein NMR spectroscopy. *Chem. Commun. 48*, 10681−10683.
(63) Welte, H., Zhou, T., Mihajlenko, X., Mayans, O., and Kovermann, M. (2020) What does fluorine do to a protein? Thermodynamic, and highly-resolved structural insights into fluorine-labelled variants of the cold shock protein. *Sci. Rep. 10*, 2640.
(64) Evanics, F., Bezsonova, I., Marsh, J., Kitevski, J. L., Forman-Kay, J. D., and Prosser, R. S. (2006) Tryptophan solvent exposure in folded and unfolded states of an SH3 domain by $^{19}$F and $^{1}$H NMR. *Biochemistry 45*, 14120−14128.
(65) Becktel, W. J., and Schellman, J. A. (1987) Protein stability curves. *Biopolymers 26*, 1859−1877.
(66) Prabhu, N. V., and Sharp, K. A. (2005) Heat capacity in proteins. *Annu. Rev. Phys. Chem. 56*, 521−548.
(67) Wang, Y., Sarkar, M., Smith, A. E., Krois, A. S., and Pielak, G. J. (2012) Macromolecular crowding and protein stability. *J. Am. Chem. Soc. 134*, 16614−16618.
(68) Sarkar, M., Li, C., and Pielak, G. J. (2013) Soft interactions and crowding. *Biophys. Rev. 5*, 187−194.
(69) Sarkar, M., Smith, A. E., and Pielak, G. J. (2013) Impact of reconstituted cytosol on protein stability. *Proc. Natl. Acad. Sci. U. S. A. 110*, 19342.
(70) Ge, C., Lu, W., and Chen, A. (2017) Quantitative proteomic reveals the dynamic of protein profile during final oocyte maturation in zebrafish. *Biochem. Biophys. Res. Commun. 490*, 657−663.
(71) Kozlowski, L. P. (2017) Proteome-*pI*: Proteome isoelectric point database. *Nucleic Acids Res. 45*, D1112−D1116.
(72) Wang, Y., Li, C., and Pielak, G. J. (2010) Effects of proteins on protein diffusion. *J. Am. Chem. Soc. 132*, 9392−9397.
(73) Stadmiller, S. S., Aguilar, J. S., Parnham, S., and Pielak, G. J. (2020) Protein-peptide binding energetics under crowded conditions. *J. Phys. Chem. B 124*, 9297−9309.
(74) Ye, Y., Liu, X., Zhang, Z., Wu, Q., Jiang, B., Jiang, L., Zhang, X., Liu, M., Pielak, G. J., and Li, C. (2013) $^{19}$F NMR spectroscopy as a probe of cytoplasmic viscosity and weak protein interactions in living cells. *Chem. - Eur. J. 19*, 12705−12710.
(75) Nawrocki, G., Wang, P.-h., Yu, I., Sugita, Y., and Feig, M. (2017) Slow-down in diffusion in crowded protein solutions correlates with transient cluster formation. *J. Phys. Chem. B 121*, 11072−11084.
(76) Nawrocki, G., Karaboga, A., Sugita, Y., and Feig, M. (2019) Effect of protein−protein interactions and solvent viscosity on the rotational diffusion of proteins in crowded environments. *Phys. Chem. Chem. Phys. 21*, 876−883.
(77) Lagadic-Gossmann, D., Huc, L., and Lecureur, V. (2004) Alterations of intracellular pH homeostasis in apoptosis: Origins and roles. *Cell Death Differ. 11*, 953−961.
(78) Casey, J. R., Grinstein, S., and Orlowski, J. (2010) Sensors and regulators of intracellular pH. *Nat. Rev. Mol. Cell Biol. 11*, 50−61.
(79) Bhattacharya, S., and Lecomte, J. T. (1997) Temperature dependence of histidine ionization constants in myoglobin. *Biophys. J. 73*, 3241−3256.
(80) Molich, A., and Heisler, N. (2005) Determination of pH by microfluorometry: Intracellular and interstitial pH regulation in developing early-stage fish embryos (*Danio rerio*). *J. Exp. Biol. 208*, 4137−4149.
(81) Sakai, T., Tochio, H., Tenno, T., Ito, Y., Kokubo, T., Hiroaki, H., and Shirakawa, M. (2006) In-cell NMR spectroscopy of proteins inside *Xenopus laevis* oocytes. *J. Biomol. NMR 36*, 179−188.
(82) Veldman, M. B., and Lin, S. (2008) Zebrafish as a developmental model organism for pediatric research. *Pediatr. Res. 64*, 470−476.
(83) Blum, M., and Ott, T. (2019) *Xenopus*: An undervalued model organism to study and model human genetic disease. *Cells Tissues Organs 205*, 303−313.
(84) Schultz, T. W., and Dawson, D. A. (2003) Housing and husbandry of *Xenopus* for oocyte production. *Lab Animal 32*, 34−39.
(85) Kurtzman, M. S., Craig, M. P., Grizzle, B. K., and Hove, J. R. (2010) Sexually segregated housing results in improved early larval survival in zebrafish. *Lab Animal 39*, 183−189.


https://dx.doi.org/10.1021/acs.biochem.0c00922
*Biochemistry* 2021, 60, 451−459